 CMC, vol.8, no.2, pp.75-92, 2008

Peridynamic Simulation of Electromigration

Walter Gerstle[1], Stewart Silling[2], David Read[3], Vinod Tewary[4] and Richard Lehoucq[5]

Abstract: A theoretical framework, based upon the peridynamic model, is presented for analytical and computational simulation of electromigration. The framework allows four coupled physical processes to be modeled simultaneously: mechanical deformation, heat transfer, electrical potential distribution, and vacancy diffusion. The dynamics of void and crack formation, and hillock and whisker growth can potentially be modeled. The framework can potentially be applied at several modeling scales: atomistic, crystallite, multiple crystallite, and macro. The conceptual simplicity of the model promises to permit many phenomena observed in microchips, including electromigration, thermo-mechanical crack formation, and fatigue crack formation, to be analyzed in a systematic and unified manner. Interfacial behavior between dissimilar crystallites and materials can also be handled in a natural way. A computational implementation of the theoretical framework is proposed, and a one-dimensional example is presented.

Keyword: computational simulation, cracks, diffusion, electromigration, hillocks, metallic thin films, microelectromechanical systems, multiphysics, multi-scale, peridynamic, voids.

1 Introduction

Simulation of the physical behavior of the metallic thin films used to connect devices in integrated circuits is currently of high importance. In addition to thermo-mechanical straining and cracking, fatigue, and interfacial delamination, failure in integrated circuits occurs due to atomic diffusion and electromigration in metallic components causing voids that can sever interconnects and hillocks and whiskers that can cause short circuits between interconnects [Black 1967]. Physical and computational models are essential to understanding and thus preventing these various failure mechanisms.

In this paper, we focus upon mechanical, thermal, electrical, and atomic diffusion processes in solids. Various kinds of simulations of these processes are available in the literature such as meshless methods, boundary element methods, Green's function methods, finite element calculations using the continuum model and molecular dynamics based methods for atomistic models (see, for example, Chakrabarty and Cagin 2008; Yu and Reutskiy 2005; Divo and Kassab 2005; Yuan and Zhang 2006; Nishioka, Tchouikov and Fujimoto 2006; Oh, Katsube, and Brust 2007; Yang and Tewary 2008). While atomistic and molecular dynamics simulations have been employed in the past (see, for example, [Bachlechner et al. 2005; Chen, Cheng, and Hsu 2007]), such simulations, even on today's massively parallel computers, are limited to model sizes of perhaps ten million atoms for perhaps 100 picoseconds. This size/time scale is insufficient to model even a single crystallite, much less entire interconnect lines and devices in integrated circuits. Classical continuum mechanical models have also been employed [Maroudas and Gungor 2002; Kim and Lu 2006]. Classical continuum mechanics is, however, not efficacious for analysis of fields that are, or may become, manifestly discontinuous, as shown for example in Fig. 1.

We choose, therefore, to model electromigration using ideas from the peridynamic model [Silling 1998, Silling 2000, Silling 2002, Silling et al. 2007]. In contrast to classical continuum mod-

[1] University of New Mexico
[2] Sandia National Laboratories
[3] National Institute of Standards and Technology
[4] National Institute of Standards and Technology
[5] Sandia National Laboratories

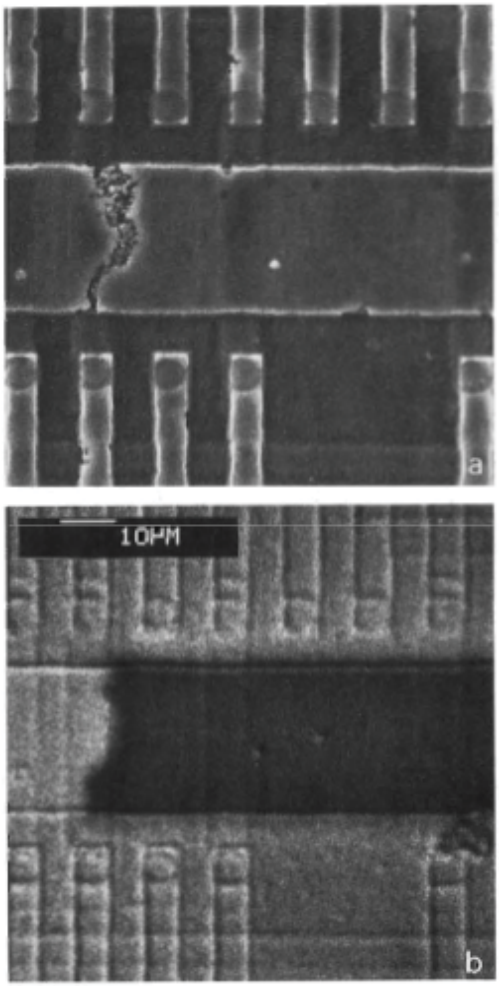

Figure 1: Open circuit induced by electromigration in an n-MOS LSI bias metallization. (a) Scanning electron micrograph. (b) Voltage contrast image. From [Scorzoni et al. 1991].

els, this model has several advantages, the foremost being that the response fields need not be continuous or differentiable. In addition, this is a potential technique for multiscale modeling since it can relate the processes at the atomistic level to observable macroscopic quantities [Tewary and Read 2004; Shen and Atluri 2004].

There is extensive literature on simulation of electromigration, see for example [Scorzoni et al. 1991]. However, as will be shown in the next section, many of the models have a limited regime of applicability and little generality or predictive capability. In this paper, our goal is to significantly broaden the regime of applicability and to simplify modeling of integrated circuits including all relevant physical mechanisms ("multi-physics modeling"). We seek to develop a modeling paradigm that can accurately predict the physical behavior of interconnects using today's computational capabilities.

The paper is organized as follows. The next section provides an overview of the physics of electromigration. We then present a section describing the state of the art of computational simulation of electromigration. Following this, we present a peridynamic multi-physics model for electromigration. We then propose a form for a multi-physics constitutive model, and a method for calibrating the peridynamic parameters. After this we provide a section describing the discretized peridynamic electromigration model of a one-dimensional example problem.

As the proposed peridynamic model is phenomenological, model parameters will need to be selected based either upon test programs or upon *ab-initio* calculations. In this paper, we propose the forms of the peridynamic models, but the model parameters must then be selected based upon the very limited available test data. It is anticipated that more physical testing will be necessary to calibrate the model parameters. Indeed, it is hoped that the proposed peridynamic multi-physics model will provide a theoretical framework for future laboratory test programs. The expectation is that once these model parameters have been calibrated through laboratory experiments, the model will be predictive for a relatively broad range of materials, geometries, and size scales.

2 The Physics of Electromigration

In this section, we provide a brief overview of the important physical models for electromigration reported in the literature, focusing on the important physical mechanisms and on the introduction of the controlling parameters that will be included below in the peridynamic model.

[Huntington and Grone 1961] describe an experiment in which a marker in the form of a scratch

on an unstressed gold wire is observed to migrate along the wire in response to applied electrical current and temperature. They created a detailed mathematical model that explains this motion as a diffusion phenomenon. Some of the model variables are not easily determined, making the model difficult to apply directly. However, the model identifies many of the significant variables and physical processes involved in electromigration.

Huntington and Grone wrote an equation in which drift velocity is linearly related to current density, with zero current density, j, coinciding with zero drift. The experiments of Blech [Blech 1976], of the type shown in Fig. 2, reveal that the relation between drift velocity and current density, although linear, is offset from the origin, as shown in Fig. 2. Blech thus proposed that

$$\begin{aligned} v_l &= \frac{D}{kT}\left[Z^* q\rho\, j - \frac{\Delta F}{l}\right] \\ &= \frac{D}{kT}\left[Z^* q\rho\, j - \frac{\Delta\sigma_{xx}\Omega}{l}\right], \end{aligned} \tag{1}$$

where v_l is the rate of drift of the strip, D is the diffusion coefficient, T is absolute temperature, k is the Boltzmann constant, Z^* is the effective charge of the diffusing atoms, q is the electron charge, ρ is the resistivity, j is the current density, l is the length of the strip, and ΔF is the difference in free energy between the two ends of the strip, which is assumed to be $\Delta F = \Omega\Delta\sigma_{xx}$, where Ω is the atomic volume and $\Delta\sigma_{xx}$ is the normal stress difference between the strip ends. The critical stress is reached when the two opposing forces are balanced, and the threshold current density, j_{cr}, to cause drift of the strip is thus

$$j_{cr} = \frac{\Delta\sigma_{xx}\Omega}{Z^* q\rho l}. \tag{2}$$

This simple model is useful in a qualitative way, but it begs several questions, such as how does one determine $\Delta\sigma_{xx}$ and j, which are, of course, fields. In this paper we seek to provide answers to these questions.

[Joo 1995] considered that the electron wind force drives an atomic (or vacancy) flux, J (with units of atoms/(m^{2}s)), given by

$$J = \left(\frac{DC}{kT}\right) Z^* qE = \left(\frac{DC}{kT}\right) Z^* q\rho\, j, \tag{3}$$

where C is the concentration of migrating species and the diffusion coefficient D varies with temperature as

$$D = D_0 \exp\left(-V/kT\right) \tag{4}$$

where V is the saddle point free energy, E is the electric field, and the remaining parameters have the same meanings as above.

Joo adds that if atoms move via grain boundary diffusion and the grain size is small compared to the line width, D should be replaced with $(\delta D_{GB}/d)$, where D_{GB} is the grain boundary diffusivity, δ is the effective width of the grain boundary, and d is the average grain diameter. One sees that there is a lack of precision about the meaning of the diffusion coefficient, D, which evidently depends upon the size scale of the interconnect and the morphology of the grain structure of the material. Joo [Joo 1995] explains that electromigration models can be classified by two approaches: the first type considers the concentration of vacancies [Shatzkes and Lloyd 1986; Kirchheim and Kaeber 1991, Nix and Arzt 1992, Clement and Lloyd 1992], and the second type considers the stress development due to migration of vacancies [Blech 1976, Korhonen *et al.* 1993]. According to Joo [Joo 1995] production and annihilation of vacancies are caused not only by the electron wind, but also by internal mechanical stresses. Thus, vacancy gradients and mechanical stress gradients are coupled.

Ogawa *et al.* [Ogawa *et al.* 2002] consider the multiple pathways that contribute to electromigration, including surface, interface, grain boundary, pipe, and lattice diffusion. Paraphrasing Ogawa *et al.*, a discussion of the various pathways allowing electromigration-related voiding can be based upon the drift equation [Vanasupa *et al.* 1999], [Hu, Rosenberg and Lee 1999]:

$$\begin{aligned} v_d &= \frac{D_{eff}}{k_B T} F_{EM,net} \\ &= \frac{D_{eff}(T)}{k_B T}\left(Z^*_{eff} e\rho\, j - \frac{\partial\sigma}{\partial x}\Omega\right). \end{aligned} \tag{5}$$

The two force contributions are the driving force due to the electron wind force, $Z^*_{eff} e\rho\, j$, and the

compensating back stress gradient from mass accumulation at the anode end of the interconnect, $\frac{\partial\sigma}{\partial x}\Omega$. Ogawa *et al.* then explain that, ignoring the back-stress component "for now", the various pathways for electromigration damage formation can be examined using the first term on the right-hand side of (5). The various pathways can be expressed as

$$Z^*_{eff}D_{eff} = Z^*_B D_B F_B + Z^*_P D_P F_P + Z^*_I D_I F_I + Z^*_S D_S F_S + Z^*_{GB} D_{GB} F_{GB}; \quad (6)$$

this relation breaks down the product of the "effective charge" and the "effective diffusivity" into its major components. The subscripts identify pathways of diffusion: $B \equiv$ bulk; $P \equiv$ pipe; $I \equiv$ interface (if it exists, in the particular interconnect); $S \equiv$ surface (if it exists); and $GB \equiv$ grain-boundary. $F_j\,(j = B,P,I,S,GB)$ is the (geometry-dependent) fraction of atoms diffusing through a given pathway.

Ogawa *et al.* go on to explain that each pathway is anticipated to have a different Z^* because the wind-force varies according to the local electronic environment surrounding a given atom [Sorbello 1996]. Because the contributions from the B and P pathways are assumed to be negligible at the temperatures of interest (400 °C), the contributions to electromigration are anticipated to arise from the I, S, and GB pathways. The model described by Ogawa *et al.* is reasonable as far as it goes, but it does not explain, for a given problem, how the fractions $F_j\,(j = B,P,I,S,GB)$ are to be assumed or computed.

In Korhonen's model [Korhonen *et al.* 1993; Joo 1995], the stress term is generalized as a local chemical potential that depends upon the hydrostatic component of the stress, σ, as:

$$\mu = \mu_0 - \Omega\sigma_V\,, \quad (7)$$

where Ω is the atomic volume (number of atoms per unit volume) and σ_V is the hydrostatic component of the stress. The chemical potential can be included in a three-dimensional peridynamic treatment of electromigration, but is not considered further here.

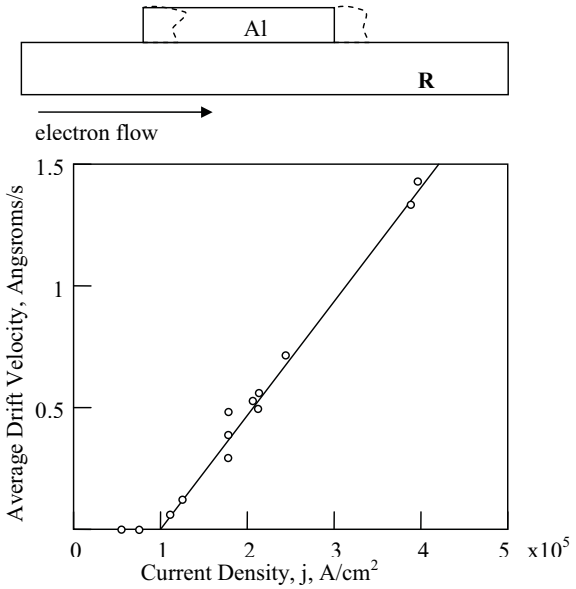

Figure 2: Experiment of Blech [Blech 1976]

3 State of the Art of Computational Simulation of Electromigration

Gungor and Maroudas [Gungor et al. 1999; Gungor and Maroudas, 2001; Maroudas and Gungor 2002] have presented a theoretical and computational model for electromigration of a single surface void on a single two-dimensional model of a thin-film crystallite, shown in Fig. 3. Their model assumes that electromigration occurs only due to adatom diffusion on the surface of the crystallite. They include crystallite anisotropy in the surface diffusion model. Their analysis is based on the continuum formalism of surface mass transport under the action of electric fields.

By computationally solving a set of equations that describe the local displacement at the void, the stress, and the electric field, by means of finite element and finite difference techniques, Gungor and Maroudas were able to simulate the evolution of the shape of the edge-void. Notice that temperature is assumed to be constant in the model.

The model of Gungor and Maroudas is the most sophisticated that we have found in the literature. Even so, it is limited to one two-dimensional crystallite at constant temperature with one surface void. We seek a more general model, applicable to multiple 3D crystallites, to be discussed in the

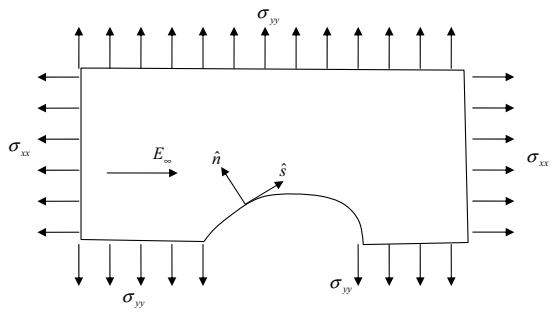

Figure 3: Schematic representation of a thin film crystallite analyzed by [Gungor and Maroudas 2001].

next section.

Our literature survey has shown that a number of electromigration models have been developed over the past 50 years. It is clear that electromigration is a process that is strongly influenced by type of metal, crystallite orientation, crystallite morphology, temperature, mechanical stress, electrical current density, dislocation density within each crystallite, and interfacial conditions with other materials. Further, all of these physical states (temperature, strain, current density, atomic concentration, *etc.*) are inextricably coupled. None of the models developed to date takes all of these complicating effects into account with any degree of generality or engineering efficacy.

Further complicating the problem is the fact that all of the models assume either continuum mechanics or atomistic representations of state. The atomistic representation is at much too small a scale to be useful for modeling of entire interconnects and vias between interconnects. The continuum mechanical models do not permit fields to evolve discontinuities; propagating cracks and evolving interfaces can be modeled only by intervening in the model, for example to release finite element nodes or to remesh to include a new surface.

Clearly, there is a need for multiphysical modeling at the meso-scale and macro-scale that allows the material state to evolve in nonlinear, dynamical ways. Such a model is presented in the next section.

4 Peridynamic Multi-Physics Model for Electromigration

4.1 Enumeration of physical mechanisms involved in electromigration

At least four physical mechanisms (and possibly more) are necessary to correctly characterize the electromigration problem: solid mechanics, heat transport, flow of electrical charge and variation of the electric field, and atomic (or vacancy) diffusion. Adding to the difficulty of the problem is the fact that these physical aspects of the problem are coupled; the term "multi-physics" seems descriptive, if not formally accurate.

In classical continuum mechanics, the forms of the differential equations governing all four of these physical phenomena are similar: in all cases, the constitutive model linearly relates a 'flux' at a point to the gradient of the conjugate field at the same point. This nomenclature implies that stress is the flux of force, which is an unfamiliar notion, but the mathematical similarities hold nonetheless. Table 1 shows the primary field, the flux, and the constitutive relation for each of the different 'physics'. The constitutive parameters are represented as constant tensors: C_{ijkl}, k_{ij}, κ_{ij}, and D_{ij}. However this assumption of linear and constant constitutive relations is a simplification, as in fact the relations between flux and the primary field variable depend nonlinearly upon the state variables, certainly in the regimes close to failure. To represent nonlinear constitutive behavior (such as plasticity and damage mechanics), C_{ijkl}, k_{ij}, κ_{ij}, and D_{ij}, become prescribed functions of the primary variables (and perhaps other state variables as well). We employ the usual convention by which summation is implied on repeated indices, so that, for example, $\frac{\partial J_i}{\partial x_i} \equiv \frac{\partial J_1}{\partial x_1} + \frac{\partial J_2}{\partial x_2} + \frac{\partial J_3}{\partial x_3}$. Subscripted indices indicating different particles will appear below as lower case Greek letters.

In addition, each mechanism or 'type of physics' involves a conservation principle involving the divergence of its respective flux, as shown in the last row of Table 1. The conserved quantities are, respectively, momentum, heat energy, electrical charge, and number of atoms. In classical con-

tinuum mechanics, the conservation equation is assumed to hold true at every point within a specified domain with a well defined boundary. Each of the conservation equations is solved subject to boundary conditions specified on the boundary of the domain.

Within traditional continuum mechanics, the problem becomes indeed very complicated when one considers that in integrated circuits there are many interacting domains with interactions across interfaces. The governing differential equations do not apply at points on these interfaces, and it is necessary to develop auxiliary equations to handle conditions on interfaces. In addition, when discontinuities in the primary fields form during the course of the solution (representing cracks and phase changes), the classical constitutive relations become undefined because the gradient of the primary field variable becomes undefined. Consequently, auxiliary types of mechanics – such as fracture mechanics – must be developed and applied. In light of these complexities involved in applying classical continuum mechanics, we propose instead to apply the methods of peridynamics, described next.

4.2 Peridynamic Solid Mechanics Model

The peridynamic multi-physics model for electromigration is a significant extension of the peridynamic solid mechanics model. The peridynamic model [Silling 1998; Silling 2000; Silling 2002; Silling 2007; Silling et al. 2007; Lehoucq and Silling 2008] makes no assumption of continuity of displacements. Thus, continuous and discontinuous (cracking and fragmentation) behavior can be handled by use of a single, simple paradigm. The method lends itself well to the modeling of quasi-brittle structures. The method is of the class of nonlocal models [Bazant and Jirasek 2002]. A major success of peridynamic solid mechanics is that discontinuities and cracks can arise in the normal operation of the model, with no need for remeshing.

The peridynamic model has no (internal) requirement for the concepts of stress and strain. The peridynamic model starts with the assumption that Newton's second law holds true on every infinitesimally small freebody (differential volume) within the domain of analysis. A force density function, called the pairwise force function (or peridynamic kernel), f, (with units of force per (unit volume)^2) between each pair of infinitesimally small particles is postulated to act if the particles are closer together than some finite distance, called the material horizon, δ. The pairwise force function may be assumed to be a function of the relative position and the relative displacement between the two particles. A spatial integration process is employed to determine the total force acting upon each particle, and a time integration process is employed to track the positions of the particles due to the applied body forces and applied displacements.

As described by Silling [Silling 1998; Silling 2000; Silling 2002; Silling *et al.* 2007], the peridynamic model may be implemented on the computer as an array of interacting discrete particles in a 3D geometrical space. One of the advantages of the peridynamic approach is that no finite element meshes are required. It is a meshless method.

Refer to Fig. 4 for terminology. We assume that Newton's second law holds true on an infinitesimally small particle, dV_α, of mass dm_α, initial or undeformed position $x_{\alpha,k}$, and displacement, $u_{\alpha,k}$, located within domain, R:

$$dm_\alpha \ddot{u}_{\alpha,k} = \sum dF_{\alpha,k}, \tag{8}$$

where $\sum dF_{\alpha,k}$ is the force vector acting on free body α, and $\ddot{u}_{\alpha,k}$ is the acceleration of particle α.

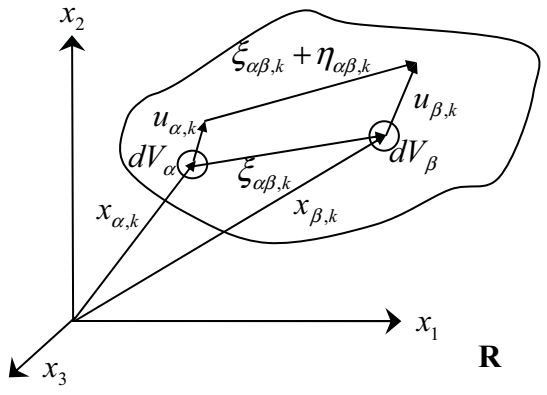

Figure 4: Terminology for peridynamic model.

Table 1: Fields and Equations in Four Types of Classical Continuum Mechanics

	Solid Mechanics	**Heat Conduction**	**Electric Conduction**	**Atomic Diffusion**
Primary Field	Displacement, $\vec{u}$	Temperature, T	Electrical Potential, Φ	Atomic (Vacancy) Concentration, C
Flux	Stress, σ_{jk}	Heat Flux, q_j	Charge Flux, j_j	Atomic Flux, J_j
Constitutive Relation	$\sigma_{ij} = \frac{C_{ijkl}}{2}\left(\frac{\partial u_k}{\partial x_l} + \frac{\partial u_l}{\partial x_k}\right)$	$q_j = -k_{jk}\frac{\partial T}{\partial x_k}$	$j_j = -\kappa_{jk}\frac{\partial \Phi}{\partial x_k}$	$J_j = -D_{jk}\frac{\partial C}{\partial x_k}$
Conservation Equation	$\frac{\partial \sigma_{ij}}{\partial x_j} + b_i = \rho \ddot{u}_i$	$\frac{\partial q_i}{\partial x_i} + \overline{Q} = c_T \rho \dot{T}$	$\frac{\partial j_i}{\partial x_i} + \overline{J} = 0$ (steady-state)	$\frac{\partial J_i}{\partial x_i} + \overline{\mathrm{K}} = c_D \dot{C}$

Definition of symbols

u_i displacement
T temperature
Φ electrical potential
C vacancy concentration (number of vacancies per total number of initial lattice sites)
σ_{ij} stress (force 'flux')
q_i heat flux
j_i electrical charge flux (electrical current density in one dimension)
J_i atomic flux
C_{ijkl} elasticity tensor
k_{ij} thermal conductivity
κ_{ij} electrical conductivity
D_{ij} diffusivity tensor
b_i applied body force per unit volume
c_T heat capacity
ρ mass density
$\overline{Q}$ rate of local introduction of heat energy
$\overline{J}$ rate of local introduction of electrical charge
c_E electrical capacitance (electrical charge per unit electrical potential per unit volume)
$\overline{K}$ rate of local introduction of atoms
c_D number of atoms per unit volume (to convert between fractional concentration and number of atoms)
Ω atomic volume

Dividing both sides of Equation 8 by the differential volume of particle α, dV_α, and partitioning the force into components internal and external to the system of particles under consideration gives

$$\rho \ddot{u}_k = L_k + b_k, \tag{9}$$

where ρ is the mass density at position x_k, L_k is the force vector per unit volume acting upon dV_α due to interaction with all other particles (for example, particle β) in domain R, and b_k is the externally applied body force vector per unit volume at position $x_{\alpha,i}$.

The interaction force density per unit volume acting upon particle α, $L_{\alpha,k}$, is an integral over all other particles, β, within the domain, R:

$$L_{\alpha,k} = \int_R \left(f_{\alpha\beta}\right)_k dV_\beta, \tag{10}$$

where $f_{\alpha\beta,k}$ is the peridynamic force vector between dV_α and dV_β. The pairwise force function, $f_{\alpha\beta,k}$, which has units of force per unit volume squared, can be viewed as a material constitutive property. In the simplest case, let us assume elastic behavior. In this case the pairwise force function:

$$\begin{aligned} f_{\alpha\beta,k} &= f_{\alpha\beta,k}\left(u_{\beta,k} - u_{\alpha,k}, x_{\beta,k} - x_{\alpha,k}\right) \\ &\equiv f_{\alpha\beta,k}\left(\eta_{\alpha\beta,k}, \xi_{\alpha\beta,k}\right), \end{aligned} \tag{11}$$

is a function of relative displacement $\eta_{\alpha\beta,k}$ and relative position $\xi_{\alpha\beta,k}$ between particles α and β. More complex constitutive relations, incorporating internal material state variables (such as damage), may also be contemplated.

Silling (Silling 1998) has proposed a simple nonlocal peridynamic constitutive model where

$$\begin{aligned} &f_{\alpha\beta,k}\left(\eta_{\alpha\beta,k}, \xi_{\alpha\beta,k}\right) = \\ &c\left[\frac{\left|\xi_{\alpha\beta,k} + \eta_{\alpha\beta,k}\right| - \left|\xi_{\alpha\beta,k}\right|}{\left|\xi_{\alpha\beta,k} + \eta_{\alpha\beta,k}\right|}\right]\left[\frac{\xi_{\alpha\beta,k} + \eta_{\alpha\beta,k}}{\left|\xi_{\alpha\beta,k} + \eta_{\alpha\beta,k}\right|}\right] \\ &= cs\hat{u} \end{aligned} \tag{12}$$

if $\left|\xi_{\alpha\beta,k} + \eta_{\alpha\beta,k}\right| - \left|\xi_{\alpha\beta,k}\right| < u^*$ and $\left|\xi_{\alpha\beta,k} + \eta_{\alpha\beta,k}\right| < \delta$; $f_{\alpha\beta,k}\left(\eta_{\alpha\beta,k}, \xi_{\alpha\beta,k}\right) = 0$ otherwise. Here c, δ, and u* are positive "microelastic" constants, s is the stretch of the bond, and $\hat{u}$ is a unit vector directed from particle α to particle β. Thus, the "spring" connecting any two particles is linear for small relative displacements, but it breaks when the relative displacement between the two particles exceeds u^*. Only particles within a distance from each other, δ (the material horizon), interact.

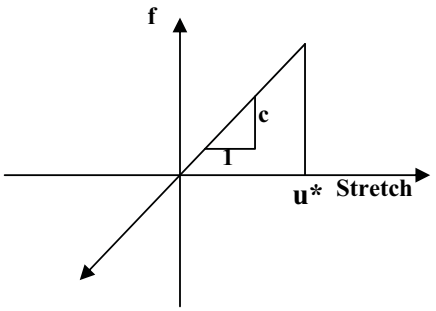

Figure 5: Micro elastic peridynamic model for quasi-brittle material. This model governs the forces between two particles situated within the material horizon, δ, of each other.

A simple micro elastic peridynamic model (with tensile limit) for brittle materials is shown in Figure 5. Recent work [Silling *et al.* 2007] has shown that the peridynamic model, employing peridynamic states (in which the pair-wise force is a function of all deformations within the material horizon), can also be used to model plasticity.

4.3 Proposed Multi-Physics Peridynamic Constitutive Model

We formulate a peridynamic model of electromigration by constructing peridynamic treatments of temperature and heat energy, electric fields and charge, and atomic flux and concentration gradients, and combining these with peridynamic solid mechanics; the present effort is the first attempt to construct a peridynamics model addressing this suite of physical mechanisms. The primary field variables (u_k, T, Φ, C) are the same as in classical continuum mechanics, as shown in the first row of Table 2. In peridynamics, integration over a material horizon replaces differentiation at a point for calculation of all of the relevant 'fluxes,' which, for electromigration, include fluxes of force, heat

energy, electrical charge, and atoms. The 'fluxes' are now nonlocal, because they are calculated by integration over a finite region, and are called the "peridynamic kernels" ($f_{F,k}$, f_q, f_j, f_J), as shown in the second row of Table 2. The peridynamic kernels have units of force, heat flow, electrical current, and atomic flow, respectively, per unit volume squared; each is a function of various primary field variables, as shown in the third row of Table 2. The functions can embody all of the constitutive behavior, including interfacial behavior between different material types and different material phases. Finally, the conservation equations, shown in the fourth row of Table 2, are applied at each material point; each involves an integral (rather than a divergence, shown in Table 1) of the peridynamic kernel over a finite neighborhood, H, at each material point.

In a peridynamic model, internal boundaries need not be explicitly defined; they are an emergent property of the base domain (which describes the geometric distribution of mass) and specified peridynamic micro-material properties. Specified primary field conditions are applied to specified regions of the base domain, and specified body forces (or the equivalent for the other physical processes: heat per unit time per unit volume; current per unit volume; atoms per unit time per unit volume) are applied to other specified regions.

The entire multi-physics constitutive model is defined by the four peridynamic kernel functions shown in Table 2: $f_{F,k}$, f_q, f_j, and f_J. These peridynamic functions define the peridynamic kernel (force, heat transfer per unit time, electrical current, and vacancy transfer per unit time, respectively) between point α and all other points, β, in terms of the (multi-physical) state of all material points within the respective material horizon of point α for each physical process: $H_{\alpha,F}$, $H_{\alpha,q}$, $H_{\alpha,j}$, and $H_{\alpha,J}$. By adopting the notation convention that the material horizon of point α, H_α, does not include point α itself, we can streamline the equations slightly.

What can we say about the form of each of these four peridynamic kernel functions? The most general form has an input domain containing all the information accessible to each point α, meaning primary fields within its material horizon H_α and for times $t \le t_c$, where t_c is the current time. The primary fields are

$$u_k\left(x_{\beta,k} \in H_{\alpha,F}, t \le t_c\right) \text{ displacement} \tag{13a}$$

$$T\left(x_{\beta,k} \in H_{\alpha,q}, t \le t_c\right) \text{ temperature} \tag{13b}$$

$$\Phi\left(x_{\beta,k} \in H_{\alpha,j}, t \le t_c\right) \text{ electrical potential} \tag{13c}$$

$$C\left(x_{\beta,k} \in H_{\alpha,J}, t \le t_c\right) \text{ atomic concentration} \tag{13d}$$

Thus, in addition to being functions of "peridynamic material attributes", the peridynamic kernels are functions of the primary fields within the peridynamic neighborhood H and the primary field histories up to time t_c:

$$f_{F,\alpha\beta,k} = f_{F,\alpha\beta,k}\Big(u_k\left(x_{\beta,k} \in H_{F,\alpha}, t \le t_c\right), T\left(x_{\beta,k} \in H_{q,\alpha}, t \le t_c\right), \Phi\left(x_{\beta,k} \in H_{j,\alpha}, t \le t_c\right), C\left(x_{\beta,k} \in H_{J,\alpha}, t \le t_c\right), t\Big) \tag{14a}$$

$$f_{q,\alpha\beta} = f_{q,\alpha\beta}\Big(u_k\left(x_{\beta,k} \in H_{F,\alpha}, t \le t_c\right), T\left(x_{\beta,k} \in H_{q,\alpha}, t \le t_c\right), \Phi\left(x_{\beta,k} \in H_{j,\alpha}, t \le t_c\right), C\left(x_{\beta,k} \in H_{J,\alpha}, t \le t_c\right), t\Big) \tag{14b}$$

$$f_{j,\alpha\beta} = f_{j,\alpha\beta}\Big(u_k\left(x_{\beta,k} \in H_{F,\alpha}, t \le t_c\right), T\left(x_{\beta,k} \in H_{q,\alpha}, t \le t_c\right), \Phi\left(x_{\beta,k} \in H_{j,\alpha}, t \le t_c\right), C\left(x_{\beta,k} \in H_{J,\alpha}, t \le t_c\right), t\Big) \tag{14c}$$

$$f_{J,\alpha\beta} = f_{J,\alpha\beta}\Big(u_k\left(x_{\beta,k} \in H_{F,\alpha}, t \le t_c\right), T\left(x_{\beta,k} \in H_{q,\alpha}, t \le t_c\right), \Phi\left(x_{\beta,k} \in H_{j,\alpha}, t \le t_c\right), C\left(x_{\beta,k} \in H_{J,\alpha}, t \le t_c\right), t\Big) \tag{14d}$$

These are extremely general functional forms, and we can reasonably make some simplifying assumptions. The assumption made in the original peridynamic model, with reasonable success, is that the peridynamic kernel between points α

and β depends only upon the state and positions of points α and β at the current time. Thus, the forms of the peridynamic functions become:

$$f_{F,\alpha\beta,k} = f_{F,\alpha\beta,k}\Big(x_{\alpha,k}, x_{\beta,k}, u_{\alpha,k}, u_{\beta,k}, T_\alpha, T_\beta, \Phi_\alpha, \Phi_\beta, C_\alpha, C_\beta\Big); \quad (15a)$$

$$f_{q,\alpha\beta} = f_{q,\alpha\beta}\Big(x_{\alpha,k}, x_{\beta,k}, u_{\alpha,k}, u_{\beta,k}, T_\alpha, T_\beta, \Phi_\alpha, \Phi_\beta, C_\alpha, C_\beta\Big); \quad (15b)$$

$$f_{j,\alpha\beta} = f_{j,\alpha\beta}\Big(x_{\alpha,k}, x_{\beta,k}, u_{\alpha,k}, u_{\beta,k}, T_\alpha, T_\beta, \Phi_\alpha, \Phi_\beta, C_\alpha, C_\beta\Big); \quad (15c)$$

$$f_{J,\alpha\beta} = f_{J,\alpha\beta}\Big(x_{\alpha,k}, x_{\beta,k}, u_{\alpha,k}, u_{\beta,k}, T_\alpha, T_\beta, \Phi_\alpha, \Phi_\beta, C_\alpha, C_\beta\Big); \quad (15d)$$

Even more simply, the assumption can be made that peridynamic kernels depend only upon the *differences* between states at the two points α and β:

$$f_{F,\alpha\beta,k} = f_{F,\alpha\beta,k}\Big(\xi_{\alpha\beta,k}, \eta_{\alpha\beta,k}, \tau_{\alpha\beta}, \varphi_{\alpha\beta}, \chi_{\alpha\beta}\Big); \quad (16a)$$

$$f_{q,\alpha\beta} = f_{q,\alpha\beta}\Big(\xi_{\alpha\beta,k}, \eta_{\alpha\beta,k}, \tau_{\alpha\beta}, \varphi_{\alpha\beta}, \chi_{\alpha\beta}\Big); \quad (16b)$$

$$f_{j,\alpha\beta} = f_{j,\alpha\beta}\Big(\xi_{\alpha\beta,k}, \eta_{\alpha\beta,k}, \tau_{\alpha\beta}, \varphi_{\alpha\beta}, \chi_{\alpha\beta}\Big); \quad (16c)$$

$$f_{J,\alpha\beta} = f_{J,\alpha\beta}\Big(\xi_{\alpha\beta,k}, \eta_{\alpha\beta,k}, \tau_{\alpha\beta}, \varphi_{\alpha\beta}, \chi_{\alpha\beta}\Big); \quad (16d)$$

where $\xi_{\alpha\beta,k}, \eta_{\alpha\beta,k}, \tau_{\alpha\beta}, \varphi_{\alpha\beta}$ and $\chi_{\alpha\beta}$ are defined in Table 2.

Finally, we must assume a parametric form for each of the functions. As a simple first step, we might assume linear forms with cut-offs, similar to the form shown in Fig. 5.

4.4 Calibration of Peridynamic Parameters

In all four physical mechanisms, we can specify peridynamic parameters that produce behavior identical to the corresponding linear classical constitutive relation. Here we show how to derive parameters appropriate for the one-dimensional case, for use later in the example problem. The extension to three dimensions is straightforward. Consider, for example, thermal diffusion from Table 2 above:

$$\int_{H_q} f_q dV + \overline{Q} = c_T \rho \dot{T}, \quad (17)$$

which, as noted in (16b) above, becomes

$$\int_{H_q} f_q \left(T\left(x'\right) - T\left(x\right), x' - x\right) dV + \overline{Q} = c_T \rho \dot{T}, \quad (18)$$

where we assume that each peridynamic bond acts like a heat conduction pathway independent of the others. If f_q is assumed to depend linearly upon the temperature drop across the bond, assuming isotropic heat conduction in the body, we can write

$$f_q(\tau, \xi) = k_0 g(|\xi|)\tau, \quad (19)$$

where k_0 is a constant, $\tau \equiv T(x') - T(x)$, $\xi \equiv x' - x$, and $g(|\xi|)$ is a prescribed function of bond length only, which vanishes outside the horizon δ. The form of $g(|\xi|)$ is essentially arbitrary if all we care about is matching bulk thermal properties, so we let $g(|\xi|) = 1$ within the material horizon. Consider a one-dimensional homogeneous body with a differentiable temperature distribution, $T(x)$, as required for a classical continuum treatment. We expand T in a Taylor series near x and form

$$\tau \equiv T\left(x'\right) - T\left(x\right) = B\left(x' - x\right) + A\frac{\left(x' - x\right)^2}{2} + \ldots. \quad (20)$$

where B and A are respectively the first and second Taylor coefficients. For the one-dimensional case the volume element is $dV = (Area)dx$. We

Table 2: Peridynamic fluxes, constitutive relations, and conservation equations for modeling electromigration

	Solid Mechanics	**Heat Conduction**	**Electric Conduction**	**Atomic Diffusion**
Primary Field	Displacement, u_k	Temperature, T	Electrical Potential, Φ	Atomic Concentration, C
Peridynamic Kernel	PD Force, $f_{F,k}$	PD Heat Flux, f_q	PD Current Flux, f_j	PD Atomic Flux, f_J
Constitutive Relation	$f_{F,k} = f_{F,k}(\xi_k, \eta_k, ...)$	$f_q = f_q(\xi_k, \tau, ...)$	$f_j = f_j(\xi_k, \phi, ...)$	$f_J = f_J(\xi_k, \chi, ...)$
Conservation Equation	$\int_{H_F} f_{F,k}\, dV + b_k = \rho \ddot{u}_k$	$\int_{H_q} f_q dV + \overline{Q} = c_T \rho \dot{T}$	$\int_{H_j} f_j dV + \overline{J} = c_E \dot{\Phi}$	$\int_{H_J} f_J dV + \overline{\mathrm{K}} = c_D \dot{C}$

Definition of symbols (see Table I for previously defined symbols):

$f_{F,k}$ (vector) peridynamic force per unit volume squared
f_q peridynamic heat flow per unit volume squared
f_j peridynamic current flow per unit volume squared
f_J peridynamic concentration flow per unit volume squared
$x_{\alpha,k}$ (vector) position of point α in reference configuration
$\xi_{\alpha\beta,k}$ (vector) relative position in reference configuration, $x_{\beta,k} - x_{\alpha,k}$
$u_{\alpha,k}$ (vector) displacement of point α in reference configuration
$\eta_{\alpha\beta,k}$ (vector) displacement difference between points α and β, $u_{\beta,k} - u_{\alpha,k}$
$\tau_{\alpha\beta}$ temperature difference between points α and β, $T_\beta - T_\alpha$
$\phi_{\alpha\beta}$ electric potential difference between points α and β, $\Phi_j - \Phi_i$
$\chi_{\alpha\beta}$ concentration difference between points α and β, $C_\beta - C_\alpha$
H_F, H_q, H_j, H_J peridynamic neighborhoods for various fluxes

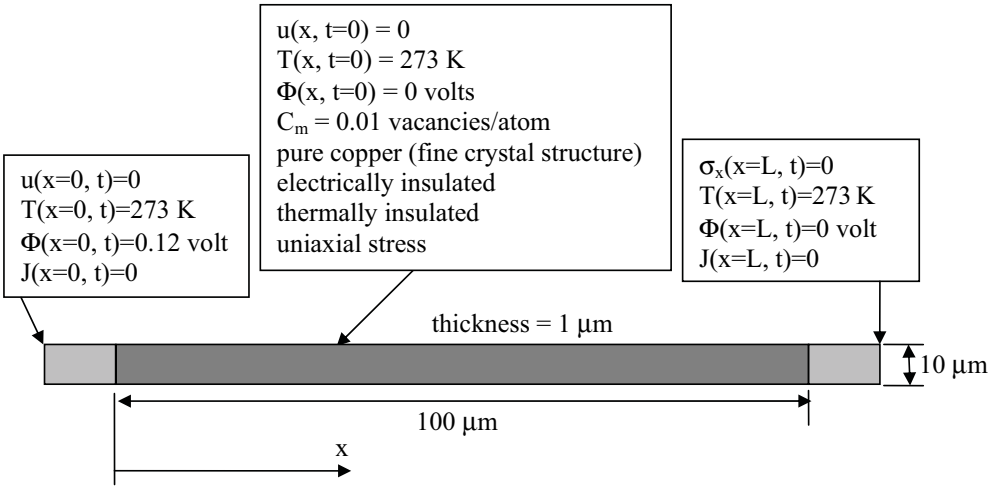

Figure 6: Thin-film copper line model, showing the boundary conditions. The active part of the line is shown in dark gray. The end sections, shown in lighter gray, are within the peridynamic material horizon of the end boundaries. They are transition regions used to isolate the active part of the model from the mathematical boundary.

extract the peridynamic result for the rate of change of temperature:

$$\begin{aligned} & c_T \rho \dot{T}(x) \\ & = \int_H k_0 g(|\xi|) \left(B\xi + A\frac{\xi^2}{2} \right) (Area)\, d\xi \\ & = k_0 (Area)\, g(|\xi|) \int_{\xi=-\delta}^{\xi=\delta} \left(B\xi + A\frac{\xi^2}{2} \right) d\xi \\ & = \frac{k_0 (Area) A \delta^3}{3} \end{aligned} \tag{21}$$

On the other hand, the classical result for the same one-dimensional temperature distribution (in the absence of a source term) is

$$\rho c_T \dot{T}(x) = k\nabla^2 T = Ak. \tag{22}$$

Equating the previous two expressions for $\rho c_T \dot{T}(x)$, we have

$$k_0 = \frac{3k}{(Area)\,\delta^3}. \tag{23}$$

Similar derivations can be employed to determine the peridynamic parameters in terms of the classical parameters for the other types of physical processes.

5 One-Dimensional Example

We present a one-dimensional example problem to demonstrate that the peridynamic approach to modeling electromigration is feasible and to show the type of results that can be obtained with a very simple treatment. The model system is a single thin-film interconnect stripe, shown in Fig. 6. The interconnect stripe is 1 μm thick, 10 μm wide, and 100 μm long. The material is copper, with a fine-grained structure compared to its dimensions. Thus, we do not model individual grains in this analysis; instead we homogenize the grains into a single "material". Carrying out such a homogenization in a realistic manner, instead of by assumption, requires detailed analysis [Lehoucq and Silling 2007].

The initial conditions and the boundary conditions at the two ends of the strip (displacement, u, temperature, T, voltage, Φ, and vacancy flux, J) are shown in Fig. 6. In addition, we assume that the strip is laterally insulated in such a way that there is no lateral stress, and no heat flux, no electrical current flux, and no vacancy flux in the lateral direction.

We assume that the cross-sectional area, A, of the stripe is a state variable that evolves with time (rather than vacancy concentration, C, which is assumed to be a function only of temperature). Specifically, we assume

$$d\dot{V} = \dot{A}dx = \left(\Omega \frac{\partial J}{\partial x} \right) A dx, \tag{24}$$

or

$$\dot{A} = \Omega A \frac{\partial J}{\partial x}, \tag{25}$$

where Ω is the atomic volume and A is the local cross-sectional area of the stripe.

The concentration of vacancies, C, is assumed to be a function of temperature only [Omar 1975]:

$$C = C_m e^{-E_v/kT}, \tag{26}$$

where C_m is the concentration of vacancies at the melting temperature of the material and E_v is the energy required to create a vacancy.

The end boundaries are held at 0°C (273 K), contrary to the usual practice in electromigration testing of heating the substrate. The sides, top, and bottom of the line are adiabatic (no heat transfer). The mechanical stress is zero, even though the line expands thermally, because the line is assumed to be mechanically unconstrained in all directions. These particular boundary conditions could be changed in a more detailed treatment. Only a single value of the diffusion constant is used here. A three-dimensional treatment could incorporate surface diffusion by applying different constitutive properties to different locations, for example by applying Eq. (6). Similarly, the behavior of grain boundaries as faster diffusion paths could be explored in the three-dimensional case by applying a different diffusion rule between volume elements within different grains.

The assumed peridynamic constitutive relations, which are particular cases of the relations given in Eqs. (16), are

$$f_{F,k} = f_{F,k}(\xi_k, \eta_k, T, C)$$

$$f_q = f_q(\xi_k, \tau, f_j)$$
$$f_j = f_j(\xi_k, \phi, ...)$$
$$f_J = f_J(\xi_k, T, C, j, \sigma).$$

The assumed classical material properties are shown in Table 3, and the derived peridynamic kernel parameters are shown in Table 4. In this analysis, we have used 30 nodes with a material horizon of 3 node spacings.

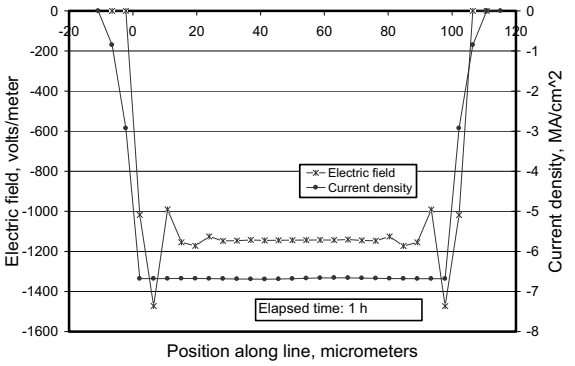

Figure 7: The negative of the electric field and current density at an elapsed time of 1 h, after the fields have stabilized. Both quantities are negative, because the electron flow is from left to right in the plot. Note the end effects, where the peridynamic boundary conditions are established. The current at this time is 0.67 A; it will change as the model evolves, because the voltage across the line is held constant. The remaining plots show only the central part of the model interconnect, from 0 to 100 μm.

Figures 7-10 show how the peridynamic fields and fluxes evolve in position and time due to electron flow from left to right along the line. In peridynamic modeling, the region of interest, from x = 0 to x = 100 μm in these plots, is surrounded by a non-physical boundary region; the boundary regions are included only in Fig. 7. We apply a negative voltage of 0.12 V within the region -10 μm $< x <$ 0 μm, to drive the electrons in the positive-x direction. Figure 7 shows the electric field and the current density as a function of position at an elapsed time of 1 h. At this time all the fluxes and fields have stabilized mathematically, but only a minimal amount of mass transport has occurred, as indicated by the small change in the line area shown in Fig. 8. The electron flow from left to right in these plots drives atoms to the right and vacancies to the left. The negative sign of the vacancy flux in Figs. 7 and 8 reflects its direction; Fig. 8 shows that the line area is already changing after only 1 h of electron flow, and that the mass transport occurs preferentially where the temperature is highest. Figure 9 shows the situation after 480 h, when the line area is reduced almost to zero. Figure 10 shows the changes with time of the maximum temperature, the maximum current density, and the minimum area. Much more detail than is displayed here can be extracted from the model. For example, the forms of the fluxes and fields shown in Figs. 7 and 8 change only slightly between 1 and 24 hours.

The present calculation is a simplified example designed to test the capabilities of the peridynamics approach to modeling electromigration. This one-dimensional example shows that peridynamics can describe in detail the evolution of an (almost) open circuit, without the need to explicitly include damage or cracking in the model. A more accurate treatment, in three dimensions, would utilize a much more detailed grid, and more realistic boundary conditions so that realistic stresses would develop. Rapid diffusion along grain boundaries and surfaces could be included in a three-dimensional treatment by assigning appropriate material constants to individual grid points.

6 Conclusions

We have presented a theoretical framework based upon the peridynamic model for analytical and computational simulation of electromigration. The framework allows four coupled physical processes to be modeled simultaneously: mechanical deformation, heat transfer, electrical potential distribution and charge flow, and vacancy diffusion. The conceptual simplicity of the model promises to permit many phenomena observed in microchips, including electromigration, thermomechanical crack formation, and fatigue crack formation, to be analyzed in a systematic and unified manner. Interfacial behavior between dissim-

Table 3: Classical Properties

Physics	Symbol	Name	Units	Value for Copper
Solid Mechanics	E	Young's modulus	N/m^2	$120x10^9$
	ν	Poisson's ratio	-	0.34
	α	coefficient of thermal expansion	1/K	$16.5x10^{-6}$
	T_m	melting temperature	K	1358
	ε_{crit}	critical elastic strain	-	0.01
	ρ	mass density	kg/m^3	8960
Thermal	k_T	thermal conductivity	J/(m·K·s)	401
	c_T	heat capacity	J/kg·K	385
Electrical	k_E	electrical conductivity	1/(m·Ohm)	$59.6x10^6$
Atomic Diffusion	m_A	atomic mass	kg/mol	$63.546x10^{-3}$
	e	elementary charge	coulomb	$1.602x10^{-19}$
	Z^*	effective atomic charge number	-	1.5
	k	Boltzmann constant	J/K	$1.3807x10^{-23}$
	Q	energy for vacancy movement	J/vacancy	$3.4877x10^{-23}$
	E_v	energy for vacancy formation	J/vacancy	$1.602x10^{-19}$
	D_0	diffusion at infinite temperature	m^2/s	$6.9x10^{-5}$
	C_m	vacancy concentration at T_m	vacancies/atom	0.01
	Ω	atomic volume	m^3	$1.182x10^{-29}$

Table 4: Constitutive Equations and Peridynamic Parameters Used in the Present One-dimensional Example, Assuming $g(|\xi|) = \left\{ \begin{matrix} 1: |\xi| \le \delta \\ 0: |\xi| > \delta \end{matrix} \right\}$

Physics	Continuum	Peridynamic kernel	Peridynamic Parameters
Solid Mechanics	$\sigma_{xx} = E\dfrac{\partial u}{\partial x}$	$f_F(\eta,\xi) = cg(\lvert\xi\rvert)s$ $= cg(\lvert\xi\rvert)\left(\dfrac{\eta}{\lvert\xi\rvert}\right)$	$c = \dfrac{2E}{(Area)\delta^2}$
Thermal	$q_x = -k_T\dfrac{\partial T}{\partial x}$	$f_T(\tau,\xi) = \kappa_T g(\lvert\xi\rvert)\tau$	$\kappa_T = \dfrac{3k_T}{(Area)\delta^3}$
Electrical	$j_x = -k_E\dfrac{\partial \Phi}{\partial x}$	$f_E(\tau,\xi) = \kappa_E g(\lvert\xi\rvert)\phi$	$\kappa_E = \dfrac{3k_E}{(Area)\delta^3}$
Atomic Vacancy Diffusion	$J_x = -\dfrac{DC}{kT}\left[\Omega\dfrac{\partial \sigma_x}{\partial x} + Z^* q\dfrac{\partial \Phi}{\partial x}\right]$	$f_C(\chi,\xi) =$ $= \dfrac{D_\xi C_\xi g(\lvert\xi\rvert)}{kT_\xi}\left[\kappa_{C\sigma}\dfrac{\Delta\sigma_x}{\lvert\xi\rvert} + \kappa_{C\Phi}\dfrac{\chi}{\lvert\xi\rvert}\right]$	$\kappa_{C\sigma} = \dfrac{2\Omega}{(Area)\delta^2}$ $\kappa_{C\Phi} = \dfrac{2Z^* q}{(Area)\delta^2}$

Notes:
Symbols are defined in Tables I, II, and III. In addition:
subscript x refers to fluxes in the positive x direction;
$\Delta\sigma_x = \sigma_{xj} - \sigma_{xi}$;
$T_\xi = \dfrac{T_\alpha + T_\beta}{2}$ is the average temperature for the link connected to nodes α and β;
$C_\xi = \dfrac{C_\alpha + C_\beta}{2}$ is the average vacancy concentration for the link connected to nodes α and β;
$D_\xi = \dfrac{D_\alpha + D_\beta}{2}$ is the average diffusivity for the link connected to nodes α and β;

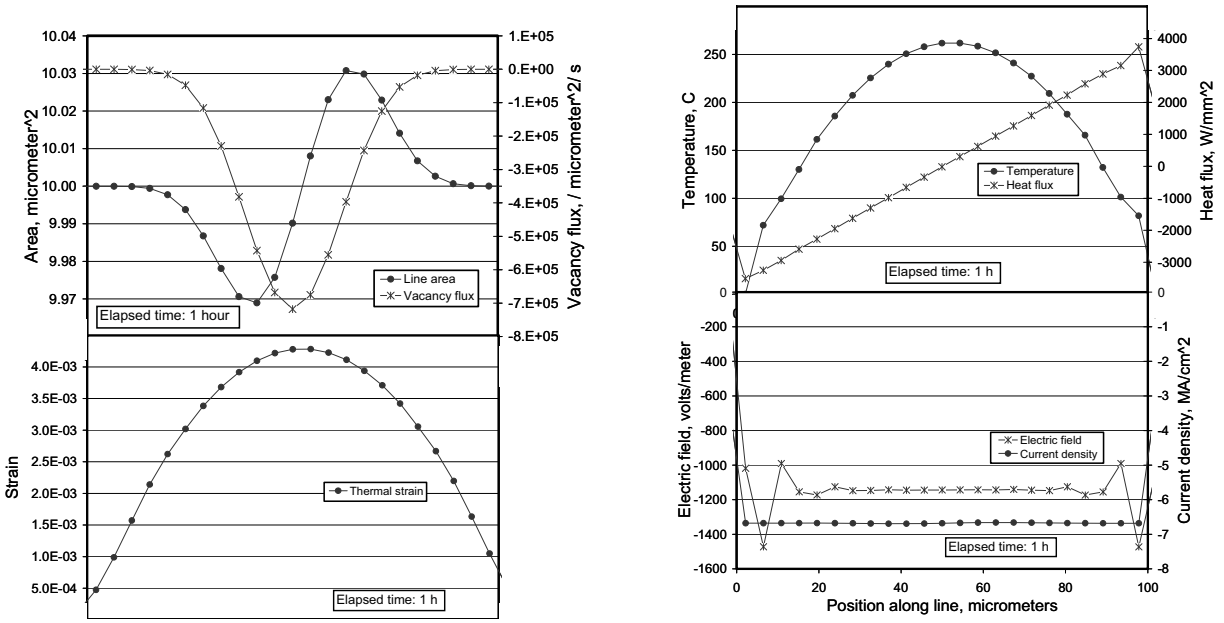

Figure 8: Quantities calculated from the one-dimensional peridynamic model at an elapsed time of 1 h: electric field, current density (right ordinate), temperature, heat flux (right ordinate), strain, line area, and vacancy flux (right ordinate). Electrons flow from left to right on these plots. The current flows from right to left, as indicated by the negative values of electric field and current density. Heat flows from the center of the line toward both ends. Atoms are driven from left to right by the electron wind, mainly near the center of the line, where the temperature is highest.

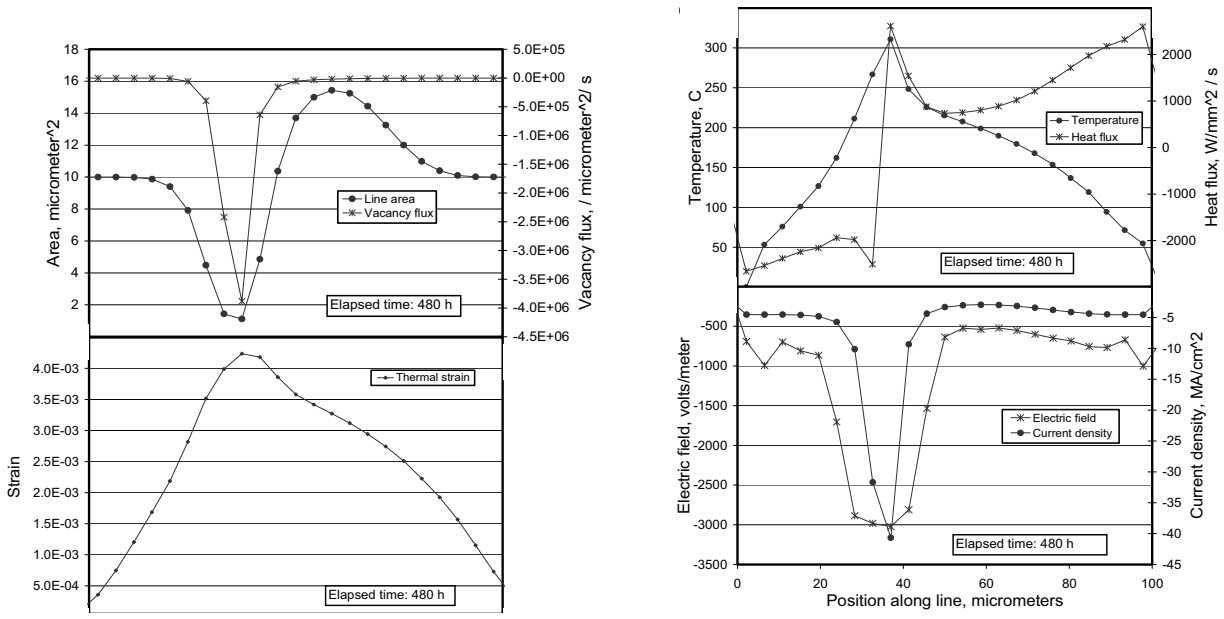

Figure 9: Quantities calculated from the one-dimensional peridynamic model at an elapsed time of 480 h. The quantities shown are as in Fig. 8. Note that the line has narrowed to an area of only slightly more than 1 square μm, and that the magnitudes of electric field and current density are much higher at the narrow region of the line than earlier in the development, before the line narrowed.

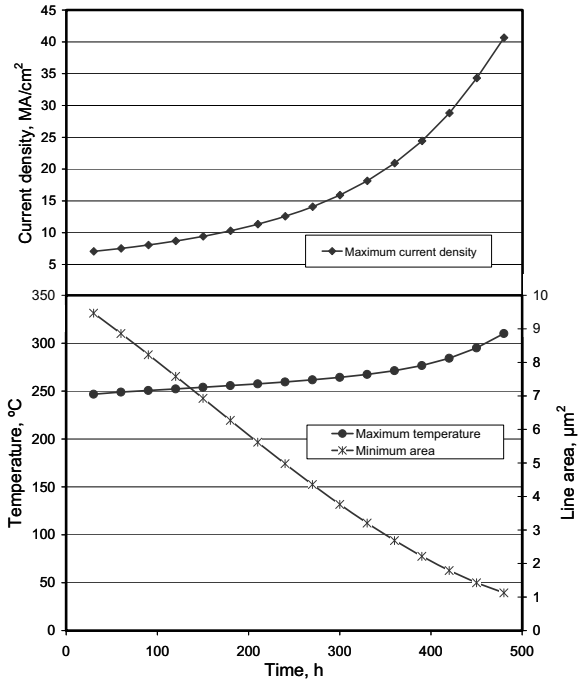

Figure 10: One-dimensional peridynamic model results for changes with time of maximum temperature, minimum line area (right-hand ordinate), and maximum current density (all at $x = 35\mu$m). The maximum temperature changes only slightly in proportion to its value, while the minimum area decreases to near zero and the maximum current density increases by a factor of over 6 between elapsed times of 1 h and 480 h.

ilar crystallites and materials can potentially be handled in a natural way.

A one-dimensional example problem employing the proposed peridynamic method has been presented. This example has demonstrated that the proposed method is capable of producing useful results even on a minimally complex model. The example demonstrates that the interdependent operation of the four physical mechanisms is simulated even as the geometry of the line changes. The results, Figs. 7-10, simulate a change in geometry driven by temperature and the electron wind, and show the effects of the geometry change on the temperature, electric field, and current density. The geometry change, which in this one-dimensional case can be visualized as a simple narrowing of the line, occurred naturally by the operation of the model.

The potential strength of the peridynamic model is in the simulation of three-dimensional problems exhibiting interfacial and cracking behavior. We hope to present the application of the peridynamic model to such examples in a future paper.

Acknowledgement: Financial support for the first author during his sabbatical leave from the University of New Mexico, the National Institute of Standards and Technology Office of Microelectronics Programs, and Sandia National Laboratories is gratefully acknowledged.

References

Bazant, Z.P.; Jirasek, M. (2002): Nonlocal Integral Formulations of Plasticity and Damage: Survey of Progress, *Journal of Engineering Mechanics*, Vol. 128, No. 11, pp. 119-149.

Bachlechner, M.E.; Zhang, J.; Wang, Ye; Schiffbauer, J.; Knudsen, S.R.; Korakakis, D. (2005): Molecular Dynamics Simulations of the Mechanical Strength of Si/Si_3N_4 Interfaces, *Physical Review B*, Vol. 72, 094115.

Black, J.R. (1967): Mass Transport of Aluminum by Momentum Exchange with Conducting Electrons, *6th Int. Reliability Phys. Symp., IEEE*, p. 148.

Blech, I.A. (1976): Electromigration in Thin Aluminum Films on Titanium Nitride, *Journal of Applied Physics*, Vol. 47, No. 4, pp. 1203-1208.

Chakrabarty, A.; Cagin, T. (2008): Computational Studies on Mechanical and Thermal Properties of Carbon Nanotube Based Nanostructures, *CMC: Computers, Materials, & Continua*, Vol. 7, No. 3, pp. 167-190.

Chen, W.H.; Cheng, H.C.; Hsu, Y.C. (2007): Mechanical Properties of Carbon Nanotubes Using Molecular Dynamics Simulations with the Inlayer van der Waals Interactions, *CMES: Computer Modeling in Engineering & Sciences*, Vol. 20, No. 2, pp. 123-146.

Clement J.J.; Lloyd J.R. (1992): Numerical Investigations of the Electromigration Boundary Value Problem, *J. Appl. Phys. Vol.* 71, p. 1729.

Divo, E.; Kassab, A.J. (2005): Transient Nonlinear Heat Conduction Solution by a Dual Reciprocity Boundary Element Method with an Effective Posteriori Error Estimator, *CMC: Computers, Materials, & Continua*, Vol.2, No.4, pp. 277-288.

Gungor, M.R.; Gray, L.J.; Zhou, S.J.; Maroudas, D. (1999): Modeling of Failure in Metallic Thin Films Induced by Stress and Electromigration: A Multiscale Computational Analysis, *Mat. Res. Soc. Symp. Proc.* 538, pp. 263-268.

Gungor, M.R.; Maroudas, D. (2001): Modeling of Electromechanically-Induced Failure of Passivated Metallic Thin Films used in Device Interconnections, *International Journal of Fracture*, 109 pp. 47-68.

Hu, C.K.; Rosenberg, R.; Lee, K.Y. (1999): Electromigration Path in Cu Thin-Film Lines, *Appl. Phys. Lett.*, Vol. 74, pp. 2945-2947.

Huntington, H.B.; Grone, A.R. (1961): Current Induced Marker Motion in Gold Wires, *J. Phys. Chem. Solids*, Vol. 20, Nos. 1/2, pp. 76-87.

Joo, Y.-C. (1995): *Electromigration Failure and Reliability of Single-Crystal and Polycrystalline Aluminum Interconnects for Integrated Circuits*, Ph.D. Thesis, MIT.

Kim, D.; Lu, W. (2006): Creep Flow, Diffusion, and Electromigration in Small Scale Interconects, *J. Mech. and Phys. of Solids*, Elsevier, Vol. 54, pp. 2554-2568.

Kirchheim, R.; Kaeber, U. (1991): Atomistic and Computer Modeling of Metallization Failure of Integrated Circuits by Electromigration, *J. Appl. Phys.*, Vol. 70, p. 172.

Korhonen, M.A.; Borgesen, P.; Tu, K.N.; Li, C.-Y. (1993): Stress Evolution Due to Electromigration in Confined Metal Lines, *J. Appl. Phys.*, Vol. 73, 3790.

Lehoucq, R.B; Silling, S.A. (2007): Statistical Coarse-Graining of Molecular Dynamics into Peridynamics, Sandia Report SAND2007-6410, Albuquerque, New Mexico.

Lehoucq, R.B.; Silling, S.A. (2008): Force flux and the peridynamic stress tensor, *J. Mech. and Phys. of Solids*, Vol. 56, No. 4, pp. 1566-1577.

Maroudas, D.; Gungor, M.R. (2002): Continuum and Atomistic Modeling of Electromechanically-induced Failure in Ductile Metallic Thin Films, *Computational Materials Science*, Vol. 23, pp. 242-249.

Nix, W.D.; Arzt, E. (1992): On Void Nucleation and Growth in Metal Interconnect Lines under Electromigration Conditions, *Metall. Trans.*, Vol. 23A, p. 2007.

Nishioka, T.; Tchouikov, S.; Fujimoto, T. (2006): Numerical Investigation of the Multiple Dynamic Crack Branching Phenomena, *CMC: Computers, Materials, & Continua*, Vol. 3, No. 3, pp. 147-154.

Oh, J.; Katsube, N.; Brust F.W. (2007): Numerical Analysis of the Effect of Diffusion and Creep Flow on Cavity Growth, *CMC: Computers, Materials, & Continua*, Vol. 6, No. 3, pp. 129-158.

Ogawa, E.T.; Lee, K.-D.; Blaschke, V.A.; Ho, P.S. (2002): Electromigration Reliability Issues in Dual-Damascene Cu Interconnections, *IEEE Transactions on Reliability*, Vol. 51, No. 4, pp. 403-419.

Omar, M.A. (1975): *Elementary Solid State Physics: Principles and Applications*, Addison Wesley.

Scorzoni, A.; Neri, B.; Caprile, C.; Fantini, F. (1991): Electromigration in thin-film interconnection lines: models, methods and results, *Materials Science Reports*, North-Holland, Vol. 7, pp. 143-220.

Shatzkes, M.; Lloyd, J.R. (1986): A Model for Conductor Failure Considering Diffusion Concurrently with Electromigration Resulting in a Current Exponent of 2, *J. Appl. Phys., Vol.*, 59, No. 11, pp. 3890-3893.

Shen, S.; Atluri, S.N. (2004): Computational Nano-Mechanics and Multi-Scale Simulation, *CMC: Computers, Materials, & Continua*, Vol. 1, No. 1, pp. 59-90.

Silling, S. (1998): Reformation of Elasticity Theory for Discontinuous and Long-Range Forces. SAND98-2176, Sandia National Laboratories, Albuquerque, NM.

Silling, S. (2000): Reformulation of Elastic-

ity Theory for Discontinuities and Long-Range Forces. Journal of the Mechanics and Physics of Solids 48: 175-209.

Silling, S. (2002): Dynamic Fracture Modeling With a Meshfree Peridynamic Code. SAND2002-2959C, Sandia National Laboratories, Albuquerque, NM.

Silling, S.A.; Epton, M.; Weckner, O.; Xu, J.; Askari, E. (2007): Peridynamic States and Constitutive Modeling, *J. Elasticity*, 88, pp. 151-184.

Sorbello, R.S. (1996): Microscopic Driving Forces for Electromigration, in Mater. *Research Soc. Symp. Proc.*, Vol. 427, pp. 73-81.

Tewary, V.K.; Read D.T. (2004): Integrated Green's Function Molecular Dynamics Method for Multiscale Modeling of Nanostructures: Application to Au Nanoisland in Cu *CMES: Computer Modeling in Engineering & Sciences*, Vol.6, No.4, pp. 359-371.

Vanasupa, L.; Joo, Y.-C.; Besser, P.R.; Pramanick, S. (1999): Texture Analysis of Damascene-Fabricated Cu lines by X-Ray Diffraction and Electron Backscatter Diffraction and Its Impact on Electromigration Performance, *L. Appl. Phys.*, Vol. 85, pp. 2583-2590.

Yu, S.; Reutskiy, S. (2005): The method of fundamental solutions for eigenproblems with Laplace and biharmonic operators, *CMC: Computers, Materials, & Continua*, Vol. 2, No. 3, pp. 177-188.

Yang, B.; Tewary, V.K. (2008): Green's Function for Multilayers with Interfacial Membrane and Flexural Rigidities, *CMC: Computers, Materials, & Continua*, Vol. 8, No. 1, pp. 23-32.

Yuan, X.G.; Zhang, R.J. (2006): Nonlinear Dynamical Analysis in Incompressible Transversely Isotropic Nonlinearly Elastic Materials: Cavity Formation and Motion in Solid Spheres, *CMC: Computers, Materials, & Continua*, Vol. 3, No. 3, pp. 119-130.